Composites Part A 126 (2019) 105599

Contents lists available at ScienceDirect

Composites Part A

journal homepage: www.elsevier.com/locate/compositesa

Enhanced mechanical and thermal properties of carbon fiber-reinforced thermoplastic polyketone composites

Jaehyun Cho[a], Seoung-Ki Lee[a], Seung-Hyun Eem[b], Jeong Gook Jang[c,*], Beomjoo Yang[d,*]

[a] Institute of Advanced Composite Materials, Korea Institute of Science and Technology (KIST), 92 Chudong-ro, Bongdong-eup, Wanju-gun, Jeonbuk 55324, Republic of Korea
[b] School of Convergence and Fusion System Engineering, Kyungpook National University, 2559 Gyeongsangdae-ro, Sangju, Gyeongsangbuk-do 37224, Republic of Korea
[c] Division of Architecture and Urban Design, Institute of Urban Science, Incheon National University, 119 Academy-ro, Yeonsu-gu, Incheon 22012, Republic of Korea
[d] School of Civil Engineering, Chungbuk National University, 1 Chungdae-ro, Seowon-gu, Cheongju, Chungbuk 28644, Republic of Korea

ARTICLE INFO

Keywords:
Polyketone
Carbon fiber-reinforced composites
Thermo-mechanical characteristics
Micromechanics, Genetic algorithm

ABSTRACT

Advances in thermoplastic composites have attracted interest among researchers for the development of new high-performance and recyclable engineering plastics. Herein, a novel polyketone (PK) composite containing carbon fiber (CF), as well as its thermophysical characteristics, was investigated. PK composites with different CF contents ranging from 0 to 30 wt% were fabricated through the two-stage extruder-injection molding process. The performances of the raw and composite materials were measured by various methods, and we found that the incorporation of CF into PK enhances the thermal stability, conductivity, and mechanical properties of the composites simultaneously. To theoretically evaluate the thermomechanical characteristics of the PK composites, a series of numerical simulation was carried out. The Kapitza resistance, which was assumed to be a model constant in this study, was determined through a genetic algorithm. The predicted properties of composites with varying CF were observed to be in good qualitative agreement with the experimental results.

1. Introduction

Recently, there has been an increasing demand for high-performance thermomechanical properties in engineering plastic [1]. In particular, as automobiles and electronics have become smaller and lighter, demand for high-performance plastic has increased. Aliphatic polyketones (PKs) are a relatively new class of material that exhibits many desirable thermophysical characteristics over conventional copolymers [2]. According to the literature [3–5], the impact strength and chemical resistance of PK are 2.3 and 2.5 times better than nylon, respectively, a typical engineering plastic. PK is also known to be an ecofriendly material, because it is composed of carbon monoxide and olefin, which are the main sources of air pollution and petrochemical materials [6].

Despite these excellent physical properties and environmental friendliness, the low elastic modulus and thermal conductivity of PK have been reported to be major drawbacks. In order to overcome these issues, various groups have conducted research on composites using PK as a matrix material. PK nanocomposites embedded with nanofillers such as organoclay have been prepared by [7] through the melt-compounding method. Two kinds of organoclays have been considered, and a highly intercalated morphology was observed when the organoclays with heat stabilizer were incorporated into the PK matrix [7]. It was confirmed that the higher intercalant molecules led to a uniform dispersion of organoclay within the PK, resulting in a notable improvement in the mechanical characteristics of the composites [7].

The surface characteristics of carbon nanotubes (CNTs) regarding the effective adhesion and mechanical strength of CNT/PK composites were investigated by [8]. The pristine CNTs were functionalized using the Grignard reagent and synthesized with the PK matrix. The surface-modified CNT was observed to have a better dispersion and interfacial adhesion than the pristine CNT in PK. Therefore, when the same amount of CNT was used as the filler, an improved tensile strength was confirmed with the surface-modified CNT [8]. In addition, studies on PK composite materials with graphene oxides (GOs) have been carried out [9]. It was reported in [9] that the PK nanocomposites with a very small polyamide-6-grafted GO content exhibited considerably improved mechanical properties. [10] fabricated and analyzed PK composites

* Corresponding authors at: School of Civil Engineering, Chungbuk National University, 1 Chungdae-ro, Seowon-gu, Cheongju, Chungbuk 28644, Republic of Korea (B. Yang). Division of Architecture and Urban Design, Institute of Urban Science, Incheon National University, 119 Academy-ro, Yeonsu-gu, Incheon 22012, Republic of Korea (J.G. Jang).
E-mail addresses: jangjg@inu.ac.kr (J.G. Jang), byang@cbnu.ac.kr (B. Yang).

https://doi.org/10.1016/j.compositesa.2019.105599
Received 25 May 2019; Received in revised form 24 July 2019; Accepted 19 August 2019
Available online 20 August 2019
1359-835X/

with various carbon nanofillers such as CNTs, GO, and antioxidant-grafted GO. It was observed that the antioxidant-grafted GO was quite effective in improving the thermal stabilities and mechanical properties of the PK composites [10]. Multi-scale studies have also been conducted for more accurate analysis of polymer composite materials [11,12].

From the literature, the synthesis of the PK matrix and nano-inclusions successfully improved the material properties. However, the use of nanoparticles, CNTs, and graphene as the inclusion is not desirable in terms of cost-effectiveness and product uniformity, which are the most important factors in commercialization. Hence, in this study, we have fabricated a PK composite reinforced with chopped carbon fiber (CF), which is a somewhat common and highly recyclable material. The chopped CFs were used as a filler, improving the thermomechanical characteristics of the neat PK polymer. The PK/CF mixtures were initially fabricated by a conventional extrusion process. The mixtures were then applied to an injection molding machine to produce the test specimens of CF-reinforced PK composites.

The thermomechanical characteristics of the raw materials and composites were analyzed using a universal testing machine (UTM), differential scanning calorimetry (DSC), thermal emission microscope, and thermogravimetric analysis (TGA). A Hot disk and infrared thermal camera were utilized to measure the thermal conductivity and monitor the temperature change of the composites, respectively. The fractured surface of the specimens was observed through a scanning electron microscope (SEM). The Tsai–Halpin and micromechanical equations were considered to theoretically analyze the mechanical and thermal properties of the composites. The reduction level of the aspect ratio of inclusion due to fiber cracking during composite fabrication was inferred through comparison with the Tsai–Halpin equation. In addition, the interfacial property between the filler and matrix, which has a great influence on the thermal conductivity, was considered as a model constant, Kapitza resistance. To more accurately estimate the model constants of the simulation, the Kapitza resistance was determined using the genetic algorithm (GA) technique. Through the proper understanding and reflection of the specimen characteristics, we confirmed that the proposed simulation correctly predicts the experimental values.

2. Methods

2.1. Materials and fabrication

Aliphatic PK (T_g and T_m are 10 and 220 °C, respectively; melt index of 60 g/min and density of 1.24 g/cm^3) was received from Hyosung (Korea). Chopped CF (T300 grade) was obtained from Toray (Japan) and used as received. The average length of the chopped CF was 6 mm and its density based on the datasheet provided was 1.76 g/cm^3. The average diameter of each CF is known to be 7 μm.

The CF and PK were prepared in a completely dried condition in a vacuum oven at 60 °C for 24 h. Then, the PK and CF were hand-mixed with a controlled CF weight fraction: 5, 10, 20, and 30 wt%. The premixtures were melt-blended by a twin-screw extruder (L/D = 15, PRISM TSE 16 TC, Thermo Electron) at a screw speed of 100 rpm, which is the maximum screw speed below the extruding capability of mixing 30 wt% of CF with the equipment setting. The temperature settings of each heating zone were set to 225 °C (hopper zone, zone 1), 230 °C (zones 2 to 4), and 225 °C (die zone, zone 5), where zone 1 represents the nearest heater and zone 5 is the farthest heater from the hopper. The extruded pellets were injection-molded by an injection molding machine (BOY 12A, BOY Machines) at a temperature setting of 240 °C for all heating zones, screw speed of 150 rpm, and back pressure of 8.5 bar. After all fabrication processes, the specimens were further dried in a convection oven before any tests. A more detailed description of the specimen fabrication process is illustrated in Fig. 1.

2.2. Characterization

The mechanical properties of the composites were measured by a tensile test according to the ASTM D638 with a UTM (LR10K, Lloyd, UK). For the tensile test, a dog-bone-shaped specimen based on type V was prepared and tested with a crosshead at 10 mm/min at room temperature and a 50% RH condition. The thermal properties of the PK and its composites were analyzed by DSC and TGA. DSC measurements were carried out by a calorimeter (Q20, TA Instruments, USA) at a heating rate of 10 °C/min with a nitrogen purge, and its second cycle was analyzed. TGA measurements were carried out (Q50, TA Instruments, USA) at a heating rate of 20 °C/min under nitrogen atmosphere. To observe the morphology of the fracture surface of the composites, field-emission SEM (Nova NanoSEM 450, FEI Corp., USA) was utilized. For the specimen preparation, a sputter coating machine (Ion Sputter E-1030, Hitachi High-Technologies Corp., Japan) was used with platinum as the sputtering source for 120 s under vacuum. The thermal profile of single CF was measured using thermal emission microscope (THEMOS mini, Hamamatsu, Japan), which was assembled with home-made vacuum chamber to measure the temperature of sample under high vacuum condition ($\sim 10^{-6}$ Torr) through a ZnSe viewport. The thermal conductivity of the composites was measured according to the ISO 22007-2 standard (TPS 2500 S, Hot Disk AB, Sweden). An infrared thermal camera (FLIR E3, FLIR Systems, USA) was utilized to monitor the temperature change of the composites during the time of heating and cooling. Heat accumulation and dissipation were visualized by the thermal images.

3. Results and discussion

3.1. Morphology characterization

To observe the CF network inside the polymer matrix through the extrusion process, morphology analysis was conducted by varying the CF loading. Fig. 2 shows SEM images of CFs protruding out of the polymer matrix, revealed from the fracture surface of the PK/CF composites. Compared to the neat PK fracture surface (Fig. 2a), the 10 wt% (Fig. 2b) and 30 wt% (Fig. 2c) CF-incorporated PK specimens show a lower-granularity surface morphology because of the high loading of the CF. In addition, it is apparent that each fiber was randomly pulled out rather than broken in both 10 wt% and 30 wt% PK/CF composites after the tensile test. This may be attributable to the weak interface formation between the CF and PK matrix. Although fiber pullout is mainly observed rather than fiber breakage after the tensile test, the gap between each fiber and polymer matrix is not clearly observed from the fracture surface. The interface between the CF and polymer matrix may be enhanced with further treatment of the CF.

3.2. Mechanical behavior

The mechanical reinforcement of the PK by CF was tested by the UTM, and five specimens were tested for reproducibility. First, experimental measurements and the theoretical prediction of Young's modulus for the PK/CF composites are presented in Fig. 3a. Young's modulus is the representative value for the stiffness of a material measured in a low strain range from the tensile test and is affected by the filler content and filler orientation in multi-component materials. Specifically, Young's modulus of composite materials reinforced with randomly oriented non-continuous fibers does not follow the rule of mixture, which only applies for continuous unidirectional fibers for predicting the composite modulus. Instead, Young's modulus of randomly oriented discontinuous fiber reinforced composites can be estimated by the Tsai–Halpin equation [13], defined as follows:

$$E_{random} = \frac{3}{8}E_{11} + \frac{5}{8}E_{22} \quad (1)$$

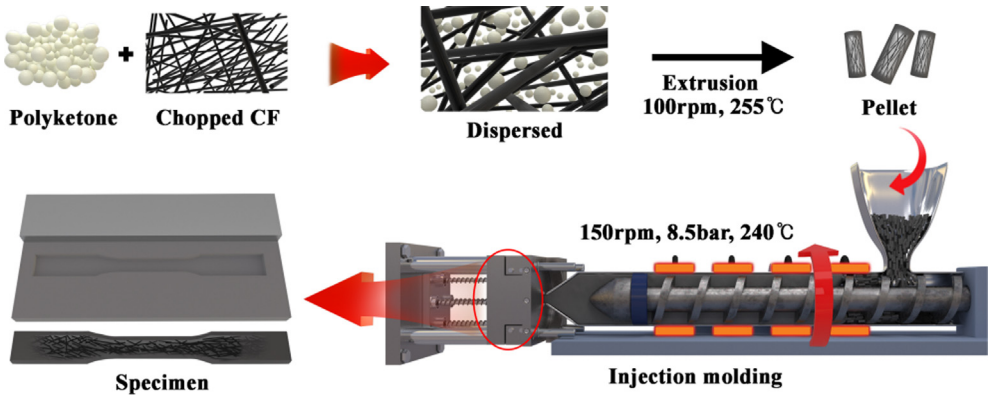

Fig. 1. Manufacturing process of carbon fiber (CF)-reinforced polyketone (PK) composites. (For interpretation of the references to colour in this figure legend, the reader is referred to the web version of this article.)

with

$$E_{11} = \frac{1+\xi\eta_L\phi_1}{1-\eta_L\phi_1}E_m,\ E_{22} = \frac{1+2\eta_T\phi_1}{1-\eta_T\phi_1}E_m,$$
$$\eta_L = \frac{(E_f/E_m)-1}{(E_f/E_m)+\xi},\ \eta_T = \frac{(E_f/E_m)-1}{(E_f/E_m)+2},\ \xi = \left(\frac{2}{3}\alpha\right) \quad (2)$$

where E_{random} is the predicted elastic modulus of the composite filled with randomly oriented discontinuous fibers, and E_m and E_f are the elastic moduli of the matrix and filler, respectively. For calculation, we take $E_m = 1.35$ GPa and $E_f = 230$ GPa. ϕ_1 and α are the volume fraction and aspect ratio of the filler, respectively.

For the experimental values, Young's modulus increases from 1.35 GPa of neat PK to 7.02 GPa of the 30 wt% CF-incorporated PK/CF composite, which shows a 520% increase in stiffness. The theoretical calculation based on the Tsai–Halpin equation was compared to the experimental results. In the extrusion and injection molding process, even though the fiber morphology was observed with SEM, it is difficult to predict the fiber breakage under high shear mixing processes. The fitted parameter in this prediction is the aspect ratio of the CF after the mixing process, and the rest of the parameters are assumed for a randomly oriented discontinuous fiber-reinforced system. The experimental Young's modulus of PK/CF composites with respect to the fiber content agrees relatively well with the prediction line, with the aspect ratio between 50 and 100. As the fiber fraction increases, the deviation between the predicted modulus and experimental values increases, which implies that the concentration of the packing defects in the composite increases with the filler fraction [14].

Fig. 3b shows the increasing trend of the tensile strength of PK/CF composites with respect to CF content. As the tensile strength of the

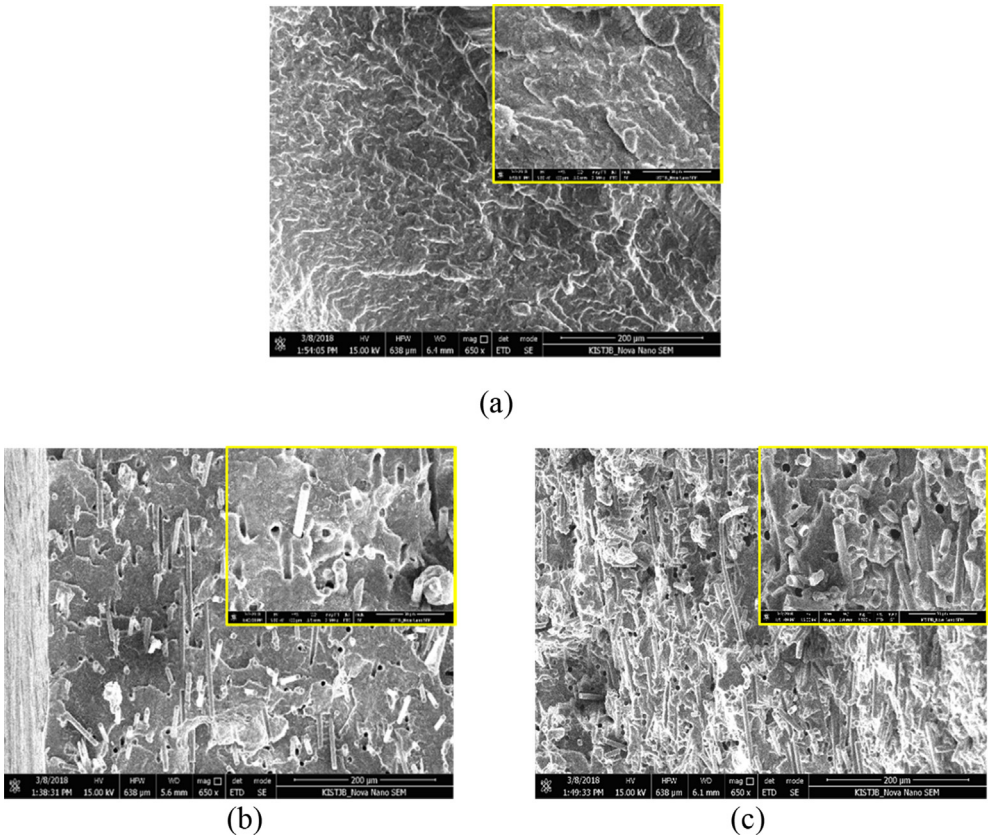

Fig. 2. SEM images of fracture surface of (a) neat PK and composites comprising (b) 10 wt% and (c) 30 wt% of CFs. (For interpretation of the references to colour in this figure legend, the reader is referred to the web version of this article.)

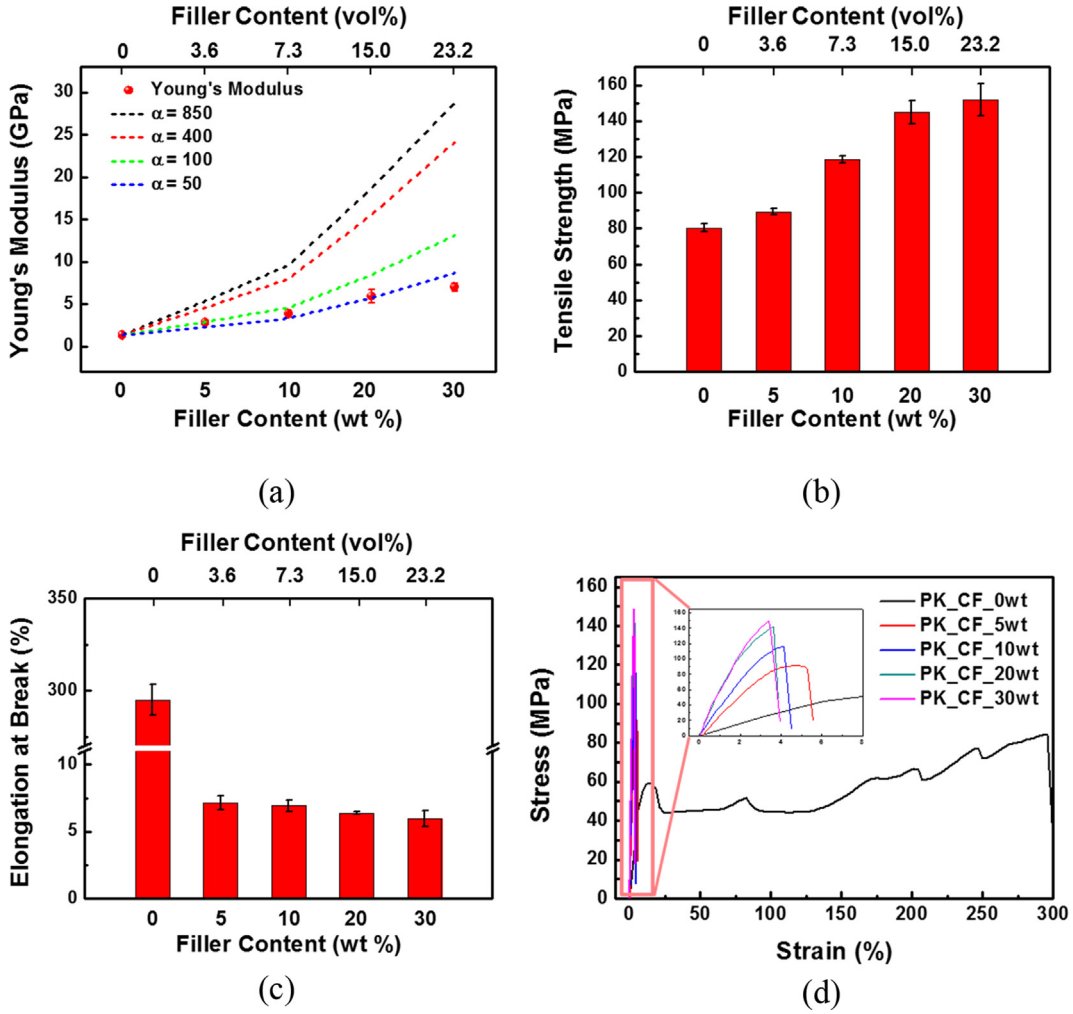

Fig. 3. The mechanical characteristics of PK composites with varying contents of CF inclusions: (a) Young's modulus, (b) tensile strength, (c) elongation at break, and (d) stress-strain curves. (For interpretation of the references to colour in this figure legend, the reader is referred to the web version of this article.)

composite is affected by interfacial interactions between the filler and polymer matrix, the results imply that the strength reinforcement by the simple mixing process is effective for PK and non-treated CF. The tensile strength of the PK/CF composites ranges from 80.33 MPa for neat PK to 151.63 MPa for the 30 wt% PK/CF composites, which shows an increase of about 189%. The elongation at break of the PK/CF composites are shown in Fig. 3c. The results follow the typical brittle fracture behavior usually present in fiber-reinforced heterogeneous composite materials. Even with a 5 wt% loading of CF, a great decrease in the elongation at break is observed in the PK/CF composites. To illustrate the overall deformational behavior of the PK/CF composites in the tensile test, the strain–stress curves are presented in Fig. 3d. These curves reveal that the PK/CF composites have a highly improved strength and stiffness compared to neat PK, and the strain decreases with CF incorporation. As shown in the inset, the magnified graph for the increasing trend of stiffness and strength for the CF-incorporated composites, and thus our composites, can be used as mechanically robust materials.

3.3. Thermal properties

As the PK is a semi-crystalline polymer, its crystallization behavior may change by incorporating CF as a reinforcing filler. To analyze the crystallization of PK/CF, thermal analysis by DSC was conducted, as shown in Fig. 4a. The values of melting temperature (T_m) and melting enthalpy change (ΔH) in the PK/CF composites with respect to the fiber content are summarized in Table 1. The T_m of the PK/CF composite ranges from 219 °C to 222 °C, which implies that there is no effective change in crystal size. In contrast, as the CF content increases, the ΔH of the PK/CF composites decreases from 77.9 J/g of neat PK to 40.8 J/g of the 30 wt% PK/CF composite, which implies that the introduction of the CF hinders the PK chain mobility, further retarding the crystal growth [15–17].

As shown in Fig. 4b, TGA analysis was conducted to observe the thermal properties of the PK/CF composites. The thermal decomposition temperature for a weight loss of 5% is 294.7 °C for neat PK, which continuously increases to 314.0 °C and then decreases to 286.1 °C for the 20 wt% and 30 wt% loaded PK/CF composites, respectively. The thermal property trend of the CF content is consistent with the DSC measurements, where the high loading of CF hinders the crystal growth and slightly affects the thermal properties. However, the change in the number of crystals and crystal size in the polymer matrix part of the composite under a high volume of CF may not have an impact on the final mechanical properties, which will be discussed in a later section. In addition, through the char yield measured by TGA, the content of the incorporated CF was experimentally measured.

The thermal conductivity of single CF, as a filler of PK/CF mixture, was measured using a self-heating method at vacuum condition (5×10^{-6} Torr). When current was applied to the CF, a temperature of fiber gradually increases due to Joule heating and temperature profile at saturated state was measured by IR camera as shown in False-color thermal image (Fig. 4c). The highest temperature was observed at

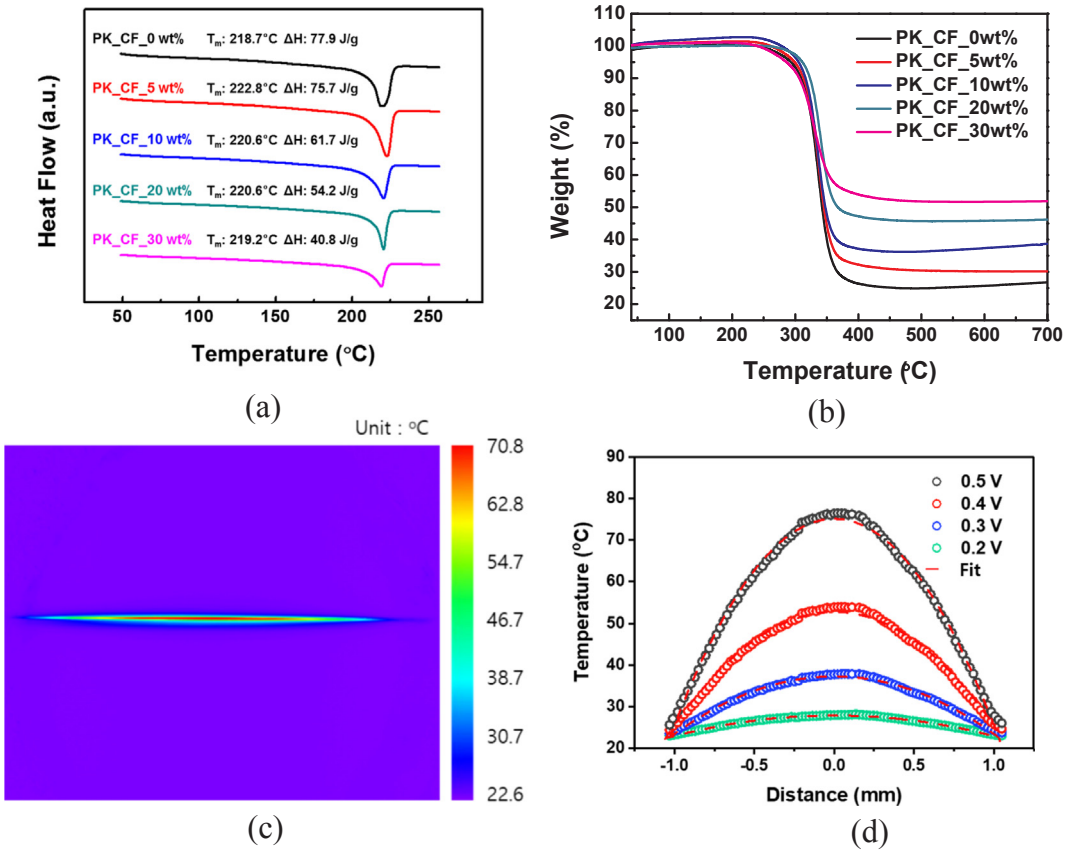

Fig. 4. The thermal analysis results of (a) differential scanning calorimetry (DSC), (b) thermogravimetric analysis (TGA), (c) false-color thermal infrared image of single CF, and (d) temperature profile along CF. (For interpretation of the references to colour in this figure legend, the reader is referred to the web version of this article.)

Table 1
The values of melting temperature (T_m) and melting enthalpy change (ΔH) in PK/CF composites with respect to the fiber content.

Sample Code	DSC		TGA	
	T_m (°C)	ΔH (J/g)	$T_{5\%}$ (°C)	Char yield (%)
PK_CF_0 wt%	218.7	77.9	294.7	24.9
PK_CF_5 wt%	222.8	75.7	298.7	29.1
PK_CF_10 wt%	220.6	61.7	304.2	34.7
PK_CF_20 wt%	220.6	54.2	314.0	46.0
PK_CF_30 wt%	219.2	40.8	286.1	51.3

middle of the fiber and the temperature decreases as it close to the edge. For the accuracy of measurement, a series of temperature profile were obtained at various applying power by increasing the voltage (Fig. 4d). Then the thermal conductivity (k) was calculated by the following equation [18],

$$T_x = T_{min}\frac{VI}{4kA_c}(L^2 - x^2) \tag{3}$$

where T_{min} is the lowest temperature at edge of fiber, VI is the applied power, A_c is the cross-sectional area of fiber, k is the thermal conductivity and L is the half length of fiber. x denotes the distance from the center of fiber. In this calculation the CF was assumed as a 1-dimensional system because the diameter of sample is much smaller than the length. The fitting curves from the theoretical calculation in Eq. (3) are matched well with experimental measurement data, which means our measurement system is highly reliable. The calculated thermal conductivity is ~10.4 W/mK, which is compatible value with a previous report [19].

3.4. Thermal performance

Fig. 5 presents the heat absorption and dissipation properties of the PK/CF composites by showing the temperature change and corresponding image by an IR camera. The transient temperature responses of Neat PK and the 10 and 30 wt% PK/CF composites on a hot plate were first observed as a temperature profile, as shown in Fig. 5a. In all samples, the speed of the increase in temperature is high in the early stage of the heating time and gradually slows down and saturates to a certain temperature. Compared to the neat PK and 10 wt% PK/CF composites, the 30 wt% PK/CF shows the fastest temperature increase and reaches the maximum temperature first; 105 °C for neat PK, 106 °C for 10 wt% PK/CF, and 111 °C for 30 wt% PK/CF. Moreover, to investigate the heat dissipation properties of the PK/CF composites, preheated samples were placed in ambient conditions to be naturally cooled down (Fig. 5b). Meanwhile, there are slight cooling speed differences among the samples; 30 wt% PK/CF, the high CF volume specimen, efficiently dissipated heat and reached the atmospheric temperature early, as expected.

Along with these results, the anisotropic thermal conductivity of the PK/CF composites with respect to CF content was measured, as shown in Fig. 6a. As expected, because of the anisotropic thermal conducting pathway of CF, the measured thermal conductivity of the PK/CF composites exhibit highly anisotropic characteristics [20]. A linear increment in thermal conductivity in the in-plane direction of the PK/CF composites is observed with respect to the CF content, while the through-plane directional thermal conductivity does not linearly increase. Although the PK/CF composite itself is composed of non-continuous randomly oriented CF, the overall thermal conductivity has an anisotropic heat transfer behavior. However, at high CF loading at

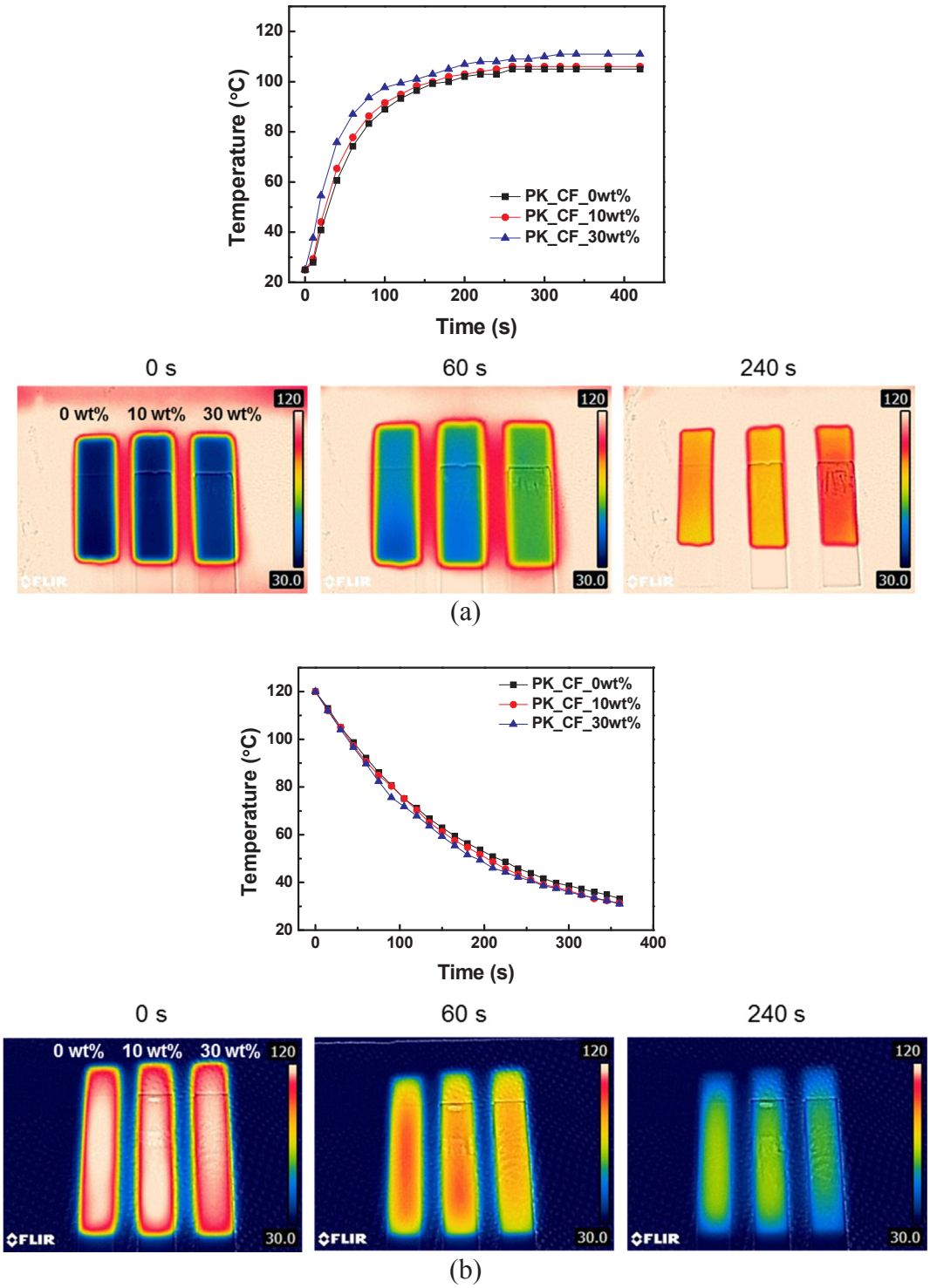

Fig. 5. The temperature profiles of PK/CF composites and corresponding photo images by IR camera on (a) heating and (b) cooling stage. (For interpretation of the references to colour in this figure legend, the reader is referred to the web version of this article.)

30 wt%, the through-plane directional thermal conductivity slightly increases because the directional randomness of the fiber increases in the confined volume.

To scrutinize the anisotropic characteristics of the thermal conductivity, we note that the micromechanics-based approach would be ideal as it can describe the microscale nature of the heterogeneous material with little empiricism. With the help of the micromechanical ensemble-volume-averaged method, the effective thermal conductivity of composites composed of the PK matrix (phase 0) and aligned CF (phase 1) is [21–23]

$$\mathbf{K}^* = \mathbf{K}_0 \cdot [\mathbf{I} + \{\phi_1 (\mathbf{A}_1 + \mathbf{S})^{-1} \cdot [\mathbf{I} - \phi_1 \mathbf{S} \cdot (\mathbf{A}_1 + \mathbf{S})^{-1}]^{-1}\}] \tag{4}$$

with [24]

$$\mathbf{A}_1 = (\mathbf{K}_1^i - \mathbf{K}_0)^{-1} \cdot \mathbf{K}_0,\ (K_{11})_1^i = \frac{K_{11}}{1 + 2R_K \frac{K_{11}}{l}},\ (K_{33})_1^i = \frac{K_{33}}{1 + 2R_K \frac{K_{33}}{d}} \tag{5}$$

where $\mathbf{I}$ denotes the identical tensor, ϕ is the volume fraction of inclusion, and the subscripts 0 and 1 denote the material phases,

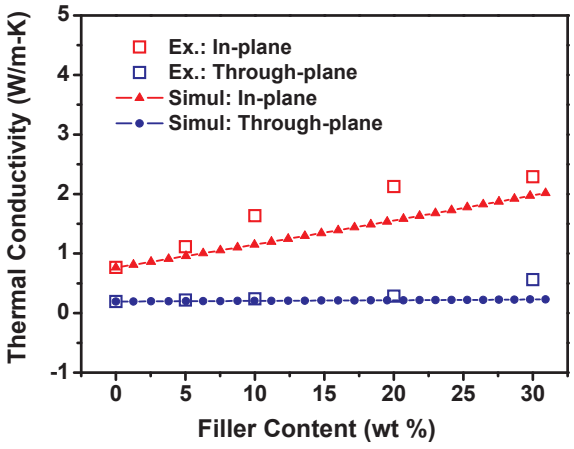

(a)

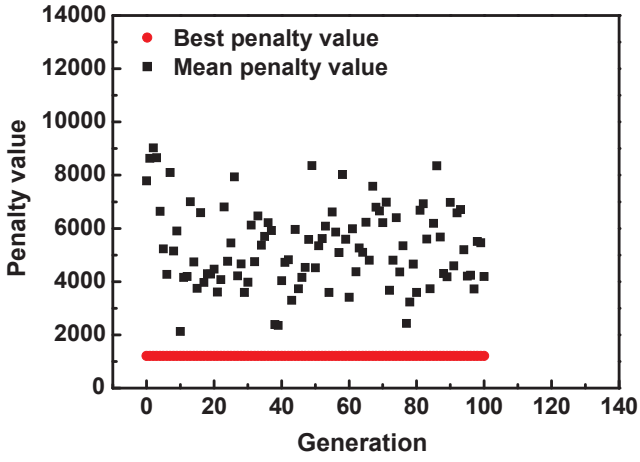

(b)

Fig. 6. (a) The experimentally measured and theoretically predicted anisotropic thermal conductivity of PK/CF composites with respect to CF content and (b) the corresponding penalty values calculated by GA. (For interpretation of the references to colour in this figure legend, the reader is referred to the web version of this article.)

indicating the matrix and inclusion, respectively [25]. **S** is Eshelby's tensor, which depends on the aspect ratio (α = length/diameter) of the CF. The components of **S** can be found in [23] and the Appendix A. R_K, l, and d are the Kapitza resistance (interfacial thermal resistance), and the length and diameter of the CF, respectively. The thermal conductivity of randomly oriented CF-reinforced PK composites can be calculated as [22,26]

$$\langle \mathbf{K}^* \rangle = \frac{1}{2\pi} \int_0^\pi \int_0^\pi l_{mi} l_{nj} \mathbf{K}^* l_{pk} l_{ql} \sin\theta \, d\theta \, d\tau \tag{6}$$

with

$$l_{mi} = \begin{bmatrix} \cos\theta & \sin\theta & 0 \\ -\sin\theta & \cos\theta & 0 \\ 0 & 0 & 1 \end{bmatrix} \tag{7}$$

The through- and in-plane thermal conductivities predicted by the above procedure are shown in Fig. 6a. The following material constants are adopted: $(\mathbf{K}_0)_{\text{Through-plane}} = 0.194$ W/mK, $(\mathbf{K}_0)_{\text{In-plane}} = 0.765$ W/mK, and $\mathbf{K}_1 = 10.4$ W/mK. The model constant of the present study, R_K, is estimated through a GA-based iteration technique. The interfacial effect is a very important factor that can change the effective properties of various composite materials [27–29]. In particular, the thermal resistance (also known as Kapitza resistance, R_K) at the interface can significantly decrease the effective conductivity of composites. In various research papers, the effects of R_K on the effective thermal conductivity of composites have been reported to be very large, and therefore we have assumed R_K as the model constant of the present theoretical analysis. The procedure for optimizing the R_K value of the simulation is shown in Table 2 [30,31]. The value of Kapitza resistance estimated via GA was R_K = 3E-8. In a physical sense, $R_K = 0$ indicates that the filler and matrix are perfectly combined; however, it is difficult for this to occur in reality. By theoretically considering the effects of the heterogeneous interface between the two materials, more realistic predictions can be made in the present study. The corresponding penalty values calculated by the GA are also illustrated in Fig. 6b.

Table 2
The procedure for optimizing Kapitza resistance (R_K).

1: Set the basic parameters for operating GA: population size, penalty rate, the maximum generation, and initialize number of generations etc.
2: Generate the initial random population of chromosome (R_K)
3: Send the initial population to Eq. (5) and test for the best initial solution by evaluating the penalty of chromosome. The penalty can be calculated by

$$F_{penalty} = \arg_{R_K} \min \sum_{i=1}^{N_{max\_gen}} (\hat{D}_i - D)^T (\hat{D}_i - D)$$

where N_{max_gen} is the maximum number of generation, $\hat{D}_i$ is the estimated thermal conductivity at the i-the chromosome, and D is the experimental data.
4: Select the best chromosome and insert into the new population.
5: Perform crossover, mutation, and check for the best chromosome. Save the best new chromosome.
6: Check the terminating condition.

4. Conclusions

In this study, the thermomechanical characteristics of a PK composite reinforced with CF were investigated experimentally and theoretically. The specimens were prepared by the extrusion-injection molding process, and the material characteristics were analyzed via various methods. The improvement in the mechanical and thermal properties according to CF content was examined. Especially, the incorporation of CFs up to 30 wt% improved the Young's modulus and thermal conductivity by approximately 520% and 300%, respectively. In this paper, the theory that can accurately predict the properties of CF-reinforced PK composites and the model constants derived from a GA are presented.

For effective commercialization, this study proposes an economical and facile manufacturing method. Based on the demonstrated improvements in thermomechanical properties by incorporating CF, it is expected that PK can be utilized as various industrial composite matrices. In particular, we found that the incorporation of CF into PK enhances the thermal stability and conductivity of the composites simultaneously. These improvements are expected be a potential solution to resolve the inherent disadvantage of PK regarding long-term thermal degradation. However, in the present study, the time-dependent and long-term characteristics of CF/PK materials were not investigated. Since we initially focused on short-term performance evaluation of PK composites, it was beyond the scope of the present paper. However, we plan to extend our work along this direction in the near future [32].

Declaration of Competing Interest

The authors declared that there is no conflict of interest.

Acknowledgement

This study was supported by Incheon National University (International Cooperative) Research Grant in 2018.

Appendix A

The Eshelby's tensor for the effective thermal conductivity ($\mathbf{K}^*$) of composites containing spheroidically shaped inclusion ($a_{11} > a_{22} = a_{33}$; $\alpha = a_{11}/a_{33}$) can be defined as:

$$(S_{11}) = 1 - \frac{\alpha}{(\alpha^2 - 1)^{1.5}}\{\alpha(\alpha^2 - 1)^{0.5} - \cosh^{-1}\alpha\},$$

$$(S_{22}) = (S_{33}) = \frac{\alpha}{2(\alpha^2 - 1)^{1.5}}\{\alpha(\alpha^2 - 1)^{0.5} - \cosh^{-1}\alpha\}, \text{ Others} = 0$$

where α ($=l/d$) is the aspect ratio.

References

[1] Haug R. The practical handbook of compost engineering. Routledge; 2018.
[2] Agostinelli E, Belli F, Tempera G, Mura A, Floris G, Toniolo L, et al. Polyketone polymer: a new support for direct enzyme immobilization. J Biotechnol 2007;127(4):670–8.
[3] Zhang Y, Broekhuis A, Stuart MC, Picchioni F. Polymeric amines by chemical modifications of alternating aliphatic polyketones. J Appl Polym Sci 2008;107(1):262–71.
[4] Zuiderduin W, Homminga D, Huétink H, Gaymans R. Influence of molecular weight on the fracture properties of aliphatic polyketone terpolymers. Polymer 2003;44(20):6361–70.
[5] Pérez-Foullerat D, Hild S, Mücke A, Rieger B. Synthesis and properties of poly (ketone-co-alcohol) materials: shape memory thermoplastic elastomers by control of the glass transition process. Macromol Chem Phys 2004;205(3):374–82.
[6] Hussein MA. Eco-friendly polythiophene (keto-amine) s based on cyclopentanone moiety for environmental remediation. J Polym Environ 2018;26(3):1194–205.
[7] Lee J, Lee KH, Kim D, Lim S, Lee S-S. Layered nanofiller-reinforced polyketone composites. Macromol Res 2013;21(11):1270–3.
[8] Nam JU, Choi EY, Park HJ, Kim C. Fabrication of polyketone-grafted multi-walled carbon nanotubes using Grignard reagent and their composites with polyketone. Compos Sci Technol 2018;167:199–205.
[9] Lim M-Y, Kim HJ, Baek SJ, Kim KY, Lee S-S, Lee J-C. Improved strength and toughness of polyketone composites using extremely small amount of polyamide 6 grafted graphene oxides. Carbon 2014;77:366–78.
[10] Lim M-Y, Oh J, Kim HJ, Kim KY, Lee S-S, Lee J-C. Effect of antioxidant grafted graphene oxides on the mechanical and thermal properties of polyketone composites. Eur Polym J 2015;69:156–67.
[11] Tam L-h, Zhou A, Yu Z, Qiu Q, Lau D. Understanding the effect of temperature on the interfacial behavior of CFRP-wood composite via molecular dynamics simulations. Compos B Eng 2017;109:227–37.
[12] Sun Q, Meng Z, Zhou G, Lin S-P, Kang H, Keten S, et al. Multi-scale computational analysis of unidirectional carbon fiber reinforced polymer composites under various loading conditions. Compos Struct 2018;196:30–43.
[13] Cho J, Jeon I, Kim SY, Lim S, Jho JY. Improving dispersion and barrier properties of polyketone/graphene nanoplatelet composites via noncovalent functionalization using aminopyrene. ACS Appl Mater Interfaces 2017;9(33):27984–94.
[14] Blumentritt BF, Vu BT, Cooper SL. Mechanical properties of discontinuous fiber reinforced thermoplastics. II. Random-in-plane fiber orientation. Polym Eng Sci 1975;15(6):428–36.
[15] Fornes T, Paul D. Crystallization behavior of nylon 6 nanocomposites. Polymer 2003;44(14):3945–61.
[16] Kim G, Yang B, Yoon H, Lee H-K. Synergistic effects of carbon nanotube and carbon fiber on heat generation and electrical characteristics of cementitious composites. Carbon 2018;134:283–92.
[17] Kim G, Yang B, Ryu G, Lee H-K. The electrically conductive carbon nanotube (CNT)/cement composites for accelerated curing and thermal cracking reduction. Compos Struct 2016;158:20–9.
[18] Xin G, Yao T, Sun H, Scott SM, Shao D, Wang G, et al. Highly thermally conductive and mechanically strong graphene fibers. Science 2015;349(6252):1083–7.
[19] Katzman HA, Adams P, Le T, Hemminger CS. Characterization of low thermal conductivity PAN-based carbon fibers. Carbon 1994;32(3):379–91.
[20] Noh YJ, Kim HS, Ku BC, Khil MS, Kim SY. Thermal conductivity of polymer composites with geometric characteristics of carbon allotropes. Adv Eng Mater 2016;18(7):1127–32.
[21] Ju J, Chen TM. Micromechanics and effective moduli of elastic composites containing randomly dispersed ellipsoidal inhomogeneities. Acta Mech 1994;103(1–4):103–21.
[22] Lee H-K, Simunovic S. Modeling of progressive damage in aligned and randomly oriented discontinuous fiber polymer matrix composites. Compos B Eng 2000;31(2):77–86.
[23] Kim SY, Jang HG, Yang C-M, Yang B. Multiscale prediction of thermal conductivity for nanocomposites containing crumpled carbon nanofillers with interfacial characteristics. Compos Sci Technol 2018;155:169–76.
[24] Nan C-W, Liu G, Lin Y, Li M. Interface effect on thermal conductivity of carbon nanotube composites. Appl Phys Lett 2004;85(16):3549–51.
[25] Yang B, Jang J-u, Eem S-H, Kim SY. A probabilistic micromechanical modeling for electrical properties of nanocomposites with multi-walled carbon nanotube morphology. Compos A Appl Sci Manuf 2017;92:108–17.
[26] Yang B, Kim B, Lee H-K. Predictions of viscoelastic strain rate dependent behavior of fiber-reinforced polymeric composites. Compos Struct 2012;94(4):1420–9.
[27] Nan C-W, Birringer R, Clarke DR, Gleiter H. Effective thermal conductivity of particulate composites with interfacial thermal resistance. J Appl Phys 1997;81(10):6692–9.
[28] Seidel GD, Lagoudas DC. A micromechanics model for the thermal conductivity of nanotube-polymer nanocomposites. J Appl Mech 2008;75(4):041025.
[29] Han Z, Fina A. Thermal conductivity of carbon nanotubes and their polymer nanocomposites: a review. Prog Polym Sci 2011;36(7):914–44.
[30] Jeon H, Yu J, Lee H, Kim G, Kim JW, Jung YC, et al. A combined analytical formulation and genetic algorithm to analyze the nonlinear damage responses of continuous fiber toughened composites. Comput Mech 2017;60(3):393–408.
[31] Sivanandam S, Deepa S. Genetic algorithm optimization problems. Introduction to genetic algorithms. Springer; 2008. p. 165–209.
[32] Yang B, Shin H, Lee H-K, Kim H. A combined molecular dynamics/micromechanics/finite element approach for multiscale constitutive modeling of nanocomposites with interface effects. Appl Phys Lett 2013;103(24):241903.